

DYNAMIC FORCE RESPONSE OF SPHERICAL HYDROSTATIC JOURNAL
BEARING FOR CRYOGENIC APPLICATIONS

Luis San Andres
Texas A&M University
College Station, Texas

522-37
12866
p. 18

ABSTRACT

Hydrostatic Journal Bearings (HJBs) are reliable and resilient fluid film rotor support elements ideal to replace roller bearings in cryogenic turbomachinery. HJBs will be used for primary space-power applications due to their long lifetime, low friction and wear, large load capacity, large direct stiffness, and damping force coefficients. An analysis for the performance characteristics of turbulent flow, orifice compensated, **spherical hydrostatic journal bearings (HJBs)** is presented. Spherical bearings allow tolerance for shaft misalignment without force performance degradation and have also the ability to support axial loads. The spherical HJB combines these advantages to provide a bearing design which could be used efficiently on high performance turbomachinery.

The motion of a barotropic liquid on the thin film bearing lands is described by bulk-flow mass and momentum equations. These equations are solved numerically using an efficient CFD method. Numerical predictions of load capacity and force coefficients for a 6 recess, spherical HJB in a LO₂ environment are presented. Fluid film axial forces and force coefficients of a magnitude about 20% of the radial load capacity are predicted for the case analyzed. Fluid inertia effects, advective and centrifugal, are found to affect greatly the static and dynamic force performance of the bearing studied.

NOMENCLATURE

A_o	$Cd \pi d_o^2/4$. Equivalent orifice area [m ²].
A_r	$1 R_r \theta_r$. Recess area [m ²].
$C_o(S), C_o, \bar{C}_o$	Radial clearance function, characteristic clearance [m], C_o/C_r .
$C_{\alpha,\beta}$	Force damping coefficients due to displacements [Ns/m], ($\alpha, \beta = X, Y, Z$)
D_r	$2 R_r$. Bearing diameter at midplane ($S=0$) [m]
d_o, C_d	Orifice diameter [m], Orifice discharge coefficient
$f_{j,B}$	$a_M [1 + (c_M r_{j,B}/H + b_M/R_{j,B})^{e_M}]$; $a_M = 0.001375$, $b_M = 500,000$ $e_M = 1/3.00$, $c_M = 10,000$, r = surface roughness
	Turbulent flow friction factors at journal and bearing surfaces.
F_X, F_Y, F_Z	Film forces along {X,Y,Z} axes [N]
f_x, f_y, f_z	$\cos\gamma, \cos\gamma, -\sin\gamma$
h_o	$H_o/c_o = C_o(s) + \epsilon_{x_o} f_x h_x + \epsilon_{y_o} f_y h_y + \epsilon_{z_o} f_z h_z$ Dimensionless zeroth-order film thickness
h_1	$\Delta\epsilon_{\alpha} f_{\alpha} h_{\alpha}$. First-order film thickness function.
h_x, h_y, h_z	$\cos\theta, \sin\theta, +1$. Circumferential film thickness components.
H_r	Recess depth [m]
$K_{\alpha,\beta}$	Force stiffness coefficients due to displacements [N/m], ($\alpha, \beta = X, Y, Z$)
L, L_R, L_L	Bearing axial length = $L_R + L_L$ [m], Right and left axial side lengths measured from recess center
l	Recess path length [m]
M	$U_{\theta} \cdot \sqrt{\beta \cdot \rho_r}$. Circumferential velocity Mach number
$M_{\alpha,\beta}$	Force inertia coefficients due to displacements [Ns ² /m], ($\alpha, \beta = X, Y, Z$)

N_{recess}	Number of recesses on bearing
P, P_s, P_r	Fluid pressure, supply and recess pressures [N/m ²]
P_o^-, P_o^+	Pressures just before and after recess edge [N/m ²]
P_L, P_R	Discharge pressures on left and right sides of bearing [N/m ²]
P_*	$\text{Min}\{P_L, P_R\}$. Characteristic discharge pressure [N/m ²]
p	$(P - P_*) / (P_o - P_*)$. Dimensionless fluid film pressure
p_x, p_y, p_z	Dimensionless dynamic (first-order) pressures
Q_{ro}	Orifice mass flow rate [kg/s].
$R(s), R_*, r(s)$	Bearing radius, Characteristic bearing radius [m], $R(s)/R_*$.
Re_c	$(\rho \Omega C R / \mu)_*$. Nominal circumferential flow Reynolds number
Re_p^*	$(\rho U C / \mu)_*$. $(C/R)_*$. Modified pressure flow Reynolds number
Re_s	$(\rho \omega C^2 / \mu)_*$. Nominal Squeeze film Reynolds number
Re_m	$(\rho U_* C / \mu)_*$. Path flow Reynolds number
R_j, R_B	$(\rho/\mu)H \sqrt{[U_\theta - \Omega \cdot R]^2 + U_s^2}$ $(\rho/\mu) H \sqrt{[U_\theta^2 + U_s^2]}$
	Flow Reynolds numbers relative to journal and bearing surfaces
S, s	Path coordinate on plane of bearing surface [m], S/R_* .
S_R, S_L	Bearing path lengths on right and left sides of bearing [m]
T_*	Fluid mean operating temperature [°K]
U_*	$C^2 \cdot (P_o - P_*) / (\mu \cdot R_*)$. Characteristic pressure flow speed [m/s]
u_s, u_θ	$(U_s, U_\theta) / U_*$. Dimensionless mean flow velocities in path (s) and circumferential (θ) directions
V_r, V_s	$(H_r + H)A_r + V_s$. Total recess volume, Volume of orifice supply line [m ³]
$\{X, Y, Z\}$	Inertial coordinate system
z	$Z(s)/R_*$. Dimensionless axial coordinate
β	$(1/\rho)(\partial\rho/\partial P)$. Liquid compressibility coefficient [m ² /N]
$\epsilon_x, \epsilon_y, \epsilon_z$	$(e_x, e_y, e_z)/C_*$. Dimensionless journal eccentricities in X, Y, Z directions
$\Delta\epsilon_x, \Delta\epsilon_y, \Delta\epsilon_z$	Dimensionless dynamic (perturbed) eccentricities
γ	Local slope of path coordinate (S) relative to Z axis
η	$H/(H_r + H)$. Ratio of land film thickness to recess depth
θ	Circumferential or angular coordinate
Θ_r	Recess angular length [rad]
$\kappa_s = \kappa_\theta$	$1/2(\kappa_j + \kappa_B)$. Turbulence shear factors in (s, θ) flow directions
κ_j, κ_B	$f_j R_j, f_B R_B$. Turbulent shear parameters at journal and bearing surfaces
κ_r	$(Re h_r)^{0.681} / 7.753$. Turbulent shear flow parameter at recess
ρ, ρ_*	Fluid density [kg/m ³], characteristic density [kg/m ³]
μ, μ_*	Fluid viscosity [Ns/m ²], characteristic viscosity [Ns/m ²]
$\xi_{\theta u}, \xi_{\theta d}$	Empirical recess-edge entrance loss coefficients in circumferential (upstream, downstream) direction
ξ_{sL}, ξ_{sR}	Empirical recess-edge entrance loss coefficients in path direction (left and right of recess)
Ω, ω	Rotational speed of journal, excitation or whirl frequency [1/s]
τ	ωt . Dimensionless time coordinate
Γ_r	Recess boundary with outward normal \bar{n} .

INTRODUCTION

Hydrostatic Journal Bearings (HJBs) are the ideal candidates to replace roller bearings as support elements in cryogenic turbomachinery. These bearings will be used for primary space-power applications due to their mechanical simplicity, long lifetime, low friction and wear, significant load capacity, and large direct stiffness as well as damping force coefficients. HJBs, unlike rolling element bearings, have no limit on a DN constraint, and shaft speeds can be allowed to increase to a level more suitable for high operating efficiency with reduced overall turbomachinery weight and size. Durability in HJBs is assured by the absence of contact between static and moving parts during steady-state operation, while long life reduces the frequency of required overhauls. Despite these attractive features, fluid film bearing stability considerations due to hydrodynamic and liquid compressibility effects are a primary concern for operation at high rotational speeds along with large pressure differentials. The present technological needs call for reliable and resilient fluid film bearing designs which provide maximum operating life with optimum - controllable rotordynamic characteristics at the lowest cost (Scharrer, 1991, 1992a).

The analysis of the flow and force response in turbulent flow hydrostatic bearings is of complex nature and confined within the realm of classical lubrication theory until recently, see for example Redecliff and Vohr (1969), Artiles et al. (1982), Chaomleffel et al. (1986). HJBs for process liquid applications present unique flow conditions, requiring for low viscosity liquids large levels of external pressurization to provide adequate load capacity and radial stiffness support. Typical pressure drops across a HJB can be as large as 30MPa and determine a fully inertial - turbulent fluid flow with significant variation of the liquid material properties across the flow region.

San Andres (1990, 1992a) introduced turbulent - inertial bulk-flow models for the analysis of compressible liquid (**barotropic**) HJBs. Extensive numerical predictions have revealed the importance of fluid inertia at the film lands and at the recess boundaries of typical high speed HJBs. San Andres (1991a) shows that moderate to large journal eccentricities have a pronounced effect on the force coefficients of HJBs with large hydrodynamic effects (high rotational speeds). Furthermore, orifice back-flow along with a sudden drop on direct stiffness are likely to occur at large eccentricity operation.

Kurtin et al. (1991), Franchek (1992), and Mosher (1993) present relevant experimental data for the static and dynamic force characteristics of water lubricated, turbulent flow, hydrostatic bearings. Experimental measurements are routinely performed for hydrostatic bearings of different geometries and at journal speeds ranging from 10,200 to 24,600 rpm and pressure supplies from 4 to 7 MPa. These references also present extensive comparisons of test results with numerical predictions based on the models of San Andres (1990, 1992a). In general the correlation between experimental and theoretical results is very good for conventional HJB geometries. It is noted that accurate theoretical results depended greatly on the knowledge of the bearing operating clearance, and most importantly, on the orifice discharge coefficients.

Adams et al. (1992) have also presented test results for the rotordynamic force coefficients of a four pad, one recess/pad, laminar flow, hydrostatic bearing. The experiments were performed with SAE 30 oil and at low rotational speeds (1000 and 2000 rpm) and low pressure supplies (max. 2.6 MPa, 375psig). Force stiffnesses and direct damping coefficients seem to be well identified while cross-coupled damping and inertia force coefficients show a rather unexpected behavior.

The threshold speed of instability and the whirl frequency ratio (WFR) define the stability characteristics of a simple rotor-bearing system. This instability is of the hydrodynamic type and solely due to the effect of journal rotational speed on the flow field. Incompressible liquid hydrostatic bearings present a whirl frequency ratio identical to that of plain journal bearings (WFR ~ 0.5). This condition,

as also verified experimentally by Mosher (1993), then limits severely the application of HJBs to high speed, light weight turbomachinery. HJBs handling highly compressible liquids, such as LH_2 for example, are prone to show a self-excited type instability of the pneumatic hammer type and can produce negative damping force coefficients for low frequency excitations. Dynamic operation under these conditions will then result in a poor stability indicator (WFR) greater than 0.50. This important result, although first reported by Redcliffe and Vohr (1969), has been largely overlooked until recently.

Recommended fixes to improve the limited dynamic stability of turbulent flow hydrostatic bearings are:

- Use of large scale roughened bearing surfaces to reduce the cross-coupled stiffness coefficients directly promoting hydrodynamic bearing instability (Franchek, 1992).
- Use of end seal restrictions or wear end-rings (Scharrer et al., 1992b) to control bearing leakage, increase the damping coefficients, and add a degree of safety for start-up and shut-down transient operation.
- Use of liquid injection opposing journal rotation to reduce the development of the circumferential flow velocity and eliminate the cross-coupled stiffness coefficient (Franchek, 1992).

The development of a leading technology in HJBs calls also for a bearing geometry not only able to provide radial load support but also with the capability to handle axial loads accompanied by shaft dynamic axial excursions (Sutton et al., 1991). Spherical bearings offer this advantage along with the capability to tolerate large levels of static and dynamic misalignment (from journal and bearing) without alteration of the bearing performance. Furthermore, the recent developments in CNC manufacturing processes allow to machine spherical surfaces almost as quickly and economically as cylindrical surfaces (Craighead, 1992).

Goenka et al. (1980) and Craighead et al. (1992) have provided analysis of spherical journal bearings for laminar/turbulent flow applications. However, in high-speed, turbulent flow applications with process liquids of low viscosity, fluid inertia effects need to be accounted. Most notably, centrifugal flow acceleration terms are of particular importance for these operating conditions. The present study considers the analysis of hemispherical hydrostatic bearings with a barotropic liquid. Turbulent bulk-flow equations of motion are derived and solved numerically using an efficient CFD algorithm. Numerical predictions for the load capacity (radial and axial) and dynamic force coefficients for a LO_2 HJB are presented and discussed in detail.

ANALYSIS

Consider, as shown in Figure 1, the flow of a variable properties liquid in the thin film region between an inner rotating journal and a stationary bearing. Cryogenic liquids are characterized by low viscosities, and thermal (energy transport) effects due to friction heating and kinetic energy variations are expected to be of minor importance in the performance of hydrostatic bearings. This assertion is not fully justified for especial operating conditions (see for example Yang et al., 1992a). On the other hand, due to the large levels of pressure differential required to provide substantial load capacity, the effects of pressure on the liquid properties, and ultimately on bearing performance, are thought to be of primary importance.

Figure 2 shows the journal outer surface as a surface of revolution formed by rotating the curve $R(Z)$ about the axis Z . The path (S) and circumferential (θ) coordinates are used as independent spatial variables. The coordinates $\{Z, R\}$ defining the journal surface are expressed as parametric functions of the path coordinate S . Trigonometric function of the angle γ defining the local slope of the path relative to the axis (Z) are given by:

$$\tan \gamma = -\frac{dR}{dZ}; \quad \sin \gamma = -\frac{dR}{dS}; \quad \cos \gamma = \frac{dZ}{dS} \quad (1)$$

where the coordinate relationships for journal/bearing spherical surfaces are:

$$\gamma = \frac{S}{R_*}; \quad R(S) = R_* \cos \gamma, \quad Z(S) = R_* \sin \gamma \quad (2)$$

and $R_*(=D_*/2)$ corresponds to the journal radius at the bearing axial midplane.

At operating conditions, the journal position relative to the bearing housing is described with reference to the inertial axes $\{X, Y, Z\}$ by the journal center displacements $(e_x(t), e_y(t), e_z(t))$. Simple geometrical relationships determine the film thickness in the flow region to be given by the following expression (Goenka et al., 1980, Childs, 1989):

$$H(S, \theta, t) = C(S) + e_x \cos \gamma \cos \theta + e_y \cos \gamma \sin \theta - e_z \sin \gamma \quad (3)$$

In a spherical bearing, journal axis rotations or misalignment provide no film thickness variation on the flow region. $C(S)$ in (3) above is a general function describing the radial clearance variation along the path coordinate for the journal centered position.

The equations of motion

The turbulent bulk-flow equations for a variable properties (**barotropic**) liquid on the thin film lands of the spherical bearing are given as (Childs, 1989):

Equation of continuity:

$$\frac{\partial}{\partial t} (\rho H) + \frac{\partial}{R \partial S} (\rho H U_s R) + \frac{\partial}{R \partial \theta} (\rho H U_\theta) = 0 \quad (4)$$

Path momentum equation

$$-H \frac{\partial P}{\partial S} = \frac{\mu}{H} (k_s U_s) + \frac{\partial (\rho H U_s)}{\partial t} + \frac{1}{R} \left\{ \frac{\partial (\rho H U_s U_s R)}{\partial S} + \frac{\partial (\rho H U_\theta U_s)}{\partial \theta} - \rho H U_\theta^2 \frac{dR}{dS} \right\} \quad (5)$$

Circumferential momentum equation:

$$-H \frac{\partial P}{R \partial \theta} = \frac{\mu}{H} \left\{ k_\theta U_\theta - k_j \frac{\Omega R}{2} \right\} + \frac{\partial (\rho H U_\theta)}{\partial t} + \frac{1}{R} \left\{ \frac{\partial (\rho H U_s U_\theta R)}{\partial S} + \frac{\partial (\rho H U_\theta U_\theta)}{\partial \theta} + \rho H U_s U_\theta \frac{dR}{dS} \right\} \quad (6)$$

on the region $\{-S_i \leq S \leq S_R; 0 \leq \theta \leq 2\pi\}$; and where, $k_* = k_\theta = (k_j + k_b)$ are the wall shear stress difference coefficients taken as local functions of the turbulent friction factors, Reynolds numbers and surface conditions, i.e, $k_j = f_j R_j$, $k_b = f_b R_b$ (Hirs, 1973, San Andres, 1992a). For inertialess-laminar fluid flows the equations above reduce to the classical form given by Goenka and Booker (1980) for spherical bearing geometries.

For cryogenic liquids such as LH2, LO2, LN2, and LCH4, the fluid properties are calculated from the Benedict-Web-Rubin equation of state as given in the standard computer program and data base of McCarty (1986).

Recess Flow and Pressure equations:

A mass conservation equation at each bearing recess of area ($l \cdot R \cdot \theta_r$) and depth H_r is defined by the global balance between the mass flow through the orifice restrictor (Q_{ro}), the mass flow into the film lands and the time rate of change of liquid mass within the recess volume V_r . This equation is given as:

$$Q_{ro} = A_o \sqrt{2\rho_r(P_s - P_R)} = \int_{\Gamma_r} \rho H (\vec{U} \cdot \vec{n}) d\Gamma_r + \rho_r \frac{\partial V_r}{\partial t} + \rho_r V_r \beta \frac{\partial P_r}{\partial t} \quad (7)$$

for $r = 1, 2, \dots, N_{recess}$

where $\beta = (1/\rho) \partial \rho / \partial P$ represents the fluid compressibility material coefficient at the recess volume, and Γ_r is the closure of the recess volume with the film lands and with normal n along the boundary line. Note that the orifice flow equation is valid only for small changes of the liquid density (Hall et al., 1986).

The fluid edge pressure at the entrance to the film lands is given by the superposition of viscous shear effects on the recess extent and an entrance drop due to fluid inertia. On the circumferential direction, the pressure rise (P_o) downstream of the recess orifice is given by (Constantinescu et al., 1987, San Andres, 1992a):

$$P_o^- = P_r - \mu_r k_r \frac{R \cdot \Theta_r}{2H_r^2} \left[U_o(\rho_o^- / \rho_r) \eta - \frac{\Omega R(s)}{2} \right] \frac{1}{(1 - M^2)} \quad (8)$$

where M is the circumferential flow local Mach number at the orifice discharge.

The entrance pressures (P_o) to the film lands in the circumferential and axial directions are given by:

$$P_o^* = P_o^- - \frac{\rho_o^*}{2} (1 + \xi_\theta) \left\{ 1 - (\rho_o^* / \rho_o^-)^2 \eta^2 \right\} U_o^2, \quad (9)$$

$$P_o^* = P_r - \frac{\rho_o^*}{2} (1 + \xi_s) \left\{ 1 - (\rho_o^* / \rho_o^-)^2 \eta^2 \right\} U_s^2 \quad (10)$$

for $r = 1, 2, \dots, N_{recess}$

The Bernoulli like pressure drop in equations (10) is considered only if the fluid leaves the recess towards the film lands. If on the contrary, fluid enters from the film lands into the bearing recess, then the edge pressure takes the value of the recess pressure (P_r). This consideration is based on momentum conservation for turbulent shear flows in sudden expansions and also on the fundamental measurements of Chaomleffel et al. (1986). The inertial pressure drop given above does not account for centrifugal flow effects in the spherical bearing geometry since the change in the bearing radial coordinate from recess edge to film lands is small.

Boundary Conditions:

Due to periodicity, the pressure and velocities are continuous and single-valued in the circumferential direction Θ ; i.e.,

$$P, U_r, U_\theta(S, \Theta, t) = P, U_r, U_\theta(S, \Theta + 2\pi, t) \quad (11)$$

At the bearing side discharge planes, the fluid pressure is equal to specified values of discharge or sump pressures, i.e.:

$$\begin{aligned} \text{at the right plane, } Z = +L_R \quad P(+S_R, \theta) &= P_R(\theta) \\ \text{at the left plane, } Z = -L_L \quad P(-S_L, \theta) &= P_R(\theta) \end{aligned} \quad (12)$$

In general the discharge pressures are uniform and constant. However, in some cryogenic turbopump applications the bearing may be located close to the pump-impeller discharge. In this case, the sump pressures are non-uniform though rotationally symmetric and expressed by a Fourier series. The boundary conditions described are valid for fluid flows well below sonic conditions.

Perturbation Analysis

Consider the journal center to describe small amplitude harmonic motions about an equilibrium static position. That is, let the journal center displacements be given as

$$e_x(t) = e_{x_0} + \Delta e_x e^{i\omega t}, \quad e_y(t) = e_{y_0} + \Delta e_y e^{i\omega t}, \quad e_z(t) = e_{z_0} + \Delta e_z e^{i\omega t}; \quad i = \sqrt{-1} \quad (13)$$

where ω denotes the frequency of the whirl motion. The magnitudes of the dynamic perturbations in journal displacements, $\{|\Delta e_x, \Delta e_y, \Delta e_z|/C_s\}$ are very small (i.e. $\ll 1$). Then, the film thickness is given by the superposition of steady-state (h_0) and dynamic (h_1) components given by the real part of the expression:

$$h = h_0 + h_1 e^{i\omega t} \quad (14a)$$

$$\text{where } h_0 = \overline{C_0}(s) + \{\epsilon_{x_0} \cos\theta + e_{y_0} \sin\theta\} \cos\gamma - \epsilon_{z_0} \sin\gamma \quad (14b)$$

$$h_1 = \Delta\epsilon_x f_x h_x + \Delta\epsilon_y f_y h_y + \Delta\epsilon_z f_z h_z \quad (14c)$$

$$\text{with } f_x(s) = f_y(s) = \cos\gamma; \quad f_z = -\sin\gamma, \quad \text{and } h_x = \cos\theta; \quad h_y = \sin\theta, \quad h_z = 1 \quad (15)$$

are the film thickness perturbed functions along the path and circumferential coordinates, respectively. These functions greatly facilitate the comprehension of the perturbed flow field equations and the resulting rotordynamic force coefficients given latter.

The flow field variables (U_r, U_θ, P), as well as the fluid properties (ρ, μ) and the shear parameters (k_θ, k_r) are also formulated as the superposition of zeroth-order and first-order complex fields describing the static equilibrium condition and the perturbed dynamic motion, respectively. In general, these fields are expressed as:

$$\Psi = \Psi_o + e^{i\tau} \{ \Delta \varepsilon_x \Psi_x + \Delta \varepsilon_y \Psi_y + \Delta \varepsilon_z \Psi_z \} = \Psi_o + e^{i\tau} \Delta \varepsilon_\alpha \Psi_\alpha, \quad \alpha = X, Y, Z \quad (16)$$

San Andres (1990,1992a) and Yang (1992b) discuss the procedure for the numerical solution of the non-linear flow equations. The differential equations of motion are integrated on staggered control volumes for each primitive variable. Program computing time is relatively small since the code uses accurate approximate analytical solutions to initiate the computational procedure and accelerate convergence to a solution defined by the operating parameters and bearing geometry.

Fluid Film Forces and Dynamic Force Coefficients

Fluid film forces are calculated by integration of the zeroth-order pressure field on the journal surface,

$$\begin{bmatrix} F_{Xo} \\ F_{Yo} \\ F_{Zo} \end{bmatrix} = (P_s - P_o) R_o^2 \int_{-s_x}^{s_x} \int_{\theta}^{\theta+2\pi} P_o \cdot \begin{bmatrix} f_x \cdot \cos\theta \\ f_y \cdot \sin\theta \\ f_z \cdot 1 \end{bmatrix} r \cdot ds \cdot d\theta \quad (17)$$

The perturbation analysis allows the dynamic force coefficients due to journal center displacements to be obtained from the general expression for dynamic forces given as:

$$\begin{bmatrix} \Delta F_x \\ \Delta F_y \\ \Delta F_z \end{bmatrix} = - \begin{bmatrix} K_{xx} & K_{xy} & K_{xz} \\ K_{yx} & K_{yy} & K_{yz} \\ K_{zx} & K_{zy} & K_{zz} \end{bmatrix} \begin{bmatrix} \Delta e_x \\ \Delta e_y \\ \Delta e_z \end{bmatrix} - \begin{bmatrix} C_{xx} & C_{xy} & C_{xz} \\ C_{yx} & C_{yy} & C_{yz} \\ C_{zx} & C_{zy} & C_{zz} \end{bmatrix} \begin{bmatrix} \Delta \dot{e}_x \\ \Delta \dot{e}_y \\ \Delta \dot{e}_z \end{bmatrix} - \begin{bmatrix} M_{xx} & M_{xy} & M_{xz} \\ M_{yx} & M_{yy} & M_{yz} \\ M_{zx} & M_{zy} & M_{zz} \end{bmatrix} \begin{bmatrix} \Delta \ddot{e}_x \\ \Delta \ddot{e}_y \\ \Delta \ddot{e}_z \end{bmatrix} \quad (18)$$

where the force coefficients due to journal center displacements are given by:

$$K_{\alpha\beta} - \omega^2 \cdot M_{\alpha\beta} + i \omega \cdot C_{\alpha\beta} = - \frac{(P_s - P_o) R_o^2}{c_o} \int_{-s_x}^{s_x} \int_{\theta}^{\theta+2\pi} p_\beta f_\alpha \cdot h_\alpha r \cdot ds d\theta \quad (19)$$

$$\alpha, \beta = X, Y, Z$$

RESULTS AND DISCUSSION

Experimental results for the steady state and dynamic force response characteristics of turbulent flow HJBs for process liquid applications are given by Kurtin et.al (1991), Adams et.al (1992), Franchek (1992), and Mosher (1993). These studies are relevant to the investigation of cylindrical bearing geometries with large pressure drops and high rotational speeds similar to those found in high performance turbomachinery components. Correlation of test measurements with predictions based on the present flow model are very favorable for smooth surface HJBs (Franchek,1992, Yang,1992b, Mosher,1993).

Spherical hydrostatic bearings may provide a unique alternative for radial load support in cryogenic liquid turbopumps (Sutton et.al, 1991) since they also offer the distinct advantages of tolerance to journal misalignment and ability to withstand shaft axial motions by providing axial thrust. In the following, the static and dynamic performance characteristics of a spherical HJB geometry handling LO₂ are presented and discussed. Normalization of results and extensive parametric studies accounting for variations in the bearing geometrical and operating parameters would be impractical due to the complex nature of the flow field and force response in turbulent hydrostatic bearings. It suffices to say that the example presented corresponds to a bearing element designed for optimal radial support at the rated operating conditions.

Table 1 shows the geometry and operating conditions of a 6 recess, LO₂ hydrostatic bearing with a fixed pressure drop across the bearing (2,000 psi) and a rotational speed equal to 22.5 Kcpm. The spherical bearing diameter (D_s) and axial length (L) are equal to 91.036 mm and 64.37 mm, respectively. The exit diameter of this bearing is equal to 64.37 mm and the arc described by the spherical path between the bearing middle and discharge planes is equal to $\gamma^* = 45^\circ$. At the rated conditions, a recess pressure ratio (P_r) equal to 0.55 provides maximum direct stiffness coefficients and requires orifices of diameter equal to 2.37 mm. Table 1 also includes values for the empirical recess-edge non - isentropic loss parameters (ξ) and orifice discharge coefficients (C_d) used in the analysis. The values chosen are representative from those used in the extensive experimental - theoretical studies of Kurtin et al. (1991) and Franchek (1992). The regime of operations of the bearings is fully turbulent with circumferential (R_{cc}) and axial flow (R_{ca}) Reynolds numbers equal to 56,900 and 35,857, respectively. A comprehensive study and comparison between the performance characteristics of equivalent cylindrical and spherical HJBs can be found in the work of San Andres (1992b).

Numerical predictions are presented for the static and dynamic force characteristics of the bearing for increasing values of the axial journal eccentricity (e_z) while the journal center is displaced radially towards the middle of the bottom recess, i.e. e_x varies and e_y=0. From equation (3), the maximum axial journal displacement is equal to $e_z = (1 - \epsilon_x \cos \gamma^*) / \sin \gamma^*$, where γ^* corresponds to the spherical angle at the bearing discharge, that is 45° for the example presented.

Figure 3 shows the radial load of the bearing as the static eccentricity (e_x) increases and for values of axial journal displacement (e_z) equal to 0.0 and 0.60, respectively. The results show the load to increase linearly with the journal lateral displacement denoting a bearing with uniform stiffness characteristics for most eccentricities. The effect of the axial journal motion is relatively small on the total bearing load. Figure 4 shows the restoring force (-F_z) as the axial journal is displaced towards the bearing shell and for increasing values of the static lateral eccentricity (e_x). The axial force appears to be linear with displacement and increases with the radial journal displacement. Note that the thrust load (F_z) is about 1/5 of the radial load, and shows the spherical bearing to have a limited axial load capacity in comparison with its radial load support.

Figures 5 and 6 show the direct (K_{xx}, K_{yy}) and cross-coupled (K_{xy}, K_{yx}) radial force stiffness coefficients, and Figure 7 presents the direct damping coefficients (C_{xx}, C_{yy}) for increasing values of the journal eccentricity e_x. The figures show the axial journal center displacements (e_z) not to affect these coefficients except at large lateral eccentricities (e_x). Note that the radial force coefficients are relatively constant for radial eccentricities as large as 50% of the bearing clearance and show clearly the major benefit of a hydrostatic bearing. A lucid discussion on the effect of these radial coefficients on the rotordynamic lateral force response can be found elsewhere (San Andres, 1991a).

Figures 8 and 9 show the direct axial stiffness (K_{zz}) and direct damping (C_{zz}) coefficients for dynamic journal axial motions as the lateral eccentricity (e_x) increases. These coefficients increase with the journal axial position and show a significant rise at moderately large radial eccentricities. At the

concentric position ($\epsilon_x = \epsilon_y = 0$), the axial stiffness is about 1/5 of the radial stiffness (K_{xx}), and the axial damping C_{zz} is approximately 11% of the direct lateral damping (C_{xx}). Thus, the axial force coefficients are relatively small when compared to the radial force coefficients. On the other hand, the magnitudes of the axial force coefficients are still significant in terms of their ability to sustain limited dynamic axial load conditions. For example, from Figure 4 it is inferred that the spherical HJB can tolerate safely an axial load as large as 5,000 N (1,125 lbs).

Cross-coupled axial force coefficients ($K_{zx}, K_{zy}, C_{zx}, C_{zy}$) due to journal lateral motions, and radial force coefficients ($K_{xz}, K_{yz}, C_{xz}, C_{yz}$) due to journal axial motions are not reproduced here for brevity. The radial force coefficients are very small except for large journal center displacements and provide a measure in uncoupling between axial dynamic motions and lateral dynamic force response. The axial force stiffness (K_{zx}, K_{zy}) are approximately 1/2 of the direct stiffness (K_{zz}) at $\epsilon_z=0.80$, $\epsilon_x=0$, and decrease rapidly as the lateral eccentricity (ϵ_x) increases.

For completeness in the analysis, calculations were performed to determine whether fluid inertia effects, both advective and centrifugal, are of importance on the static and dynamic force performance characteristics of the spherical hydrostatic bearing. Table 2 presents a summary of the results for increasing values of the journal rotational speed at the bearing concentric position ($\epsilon_x = \epsilon_y = \epsilon_z = 0$). The orifice diameter and loss coefficients are identical for the simulations. A comparison of results shows large differences on the recess pressure ratio (P_r) and the force coefficients. Fluid inertia acts as an additional flow resistance and then determines larger recess pressures with a reduced flow rate. The most notable effect is related to the reduced magnitude of the direct radial stiffnesses ($K_{xx} = K_{yy}$). At the rated operating point, 22.5 Kcpm, the values of direct stiffness are equal to 240.9 and 308.5 MN/m for the bearing with and without fluid inertia effects. This corresponds to a net reduction in hydrostatic load capacity of 22% and it is a direct consequence of the increased flow resistance due to centrifugal effects on the curved flow path and also due to the larger recess pressures. It is evident from the results presented that fluid inertia effects need to be included in the analysis of high speed, turbulent flow HJBs.

CONCLUSIONS

An analysis for the performance characteristics of turbulent flow, orifice compensated, spherical hydrostatic journal bearing (HJBs) is presented. Hydrostatic bearings offer a substantial radial load capacity and can be used with process liquids of low viscosity if large pressure differentials across the bearing are available. On the other hand, the spherical bearing geometry allows tolerance for shaft misalignment without force performance degradation and it also has the ability to support thrust loads. The spherical HJB combines these advantages to provide a bearing design which could be used efficiently on high performance turbomachinery.

The motion of a barotropic liquid on the thin film bearing lands is described by bulk-flow mass and momentum equations. Zeroth-order equations describe the fluid flow field for a journal equilibrium position, while first-order linear equations govern the fluid flow for small amplitude journal center radial and axial motions. Solution to the zeroth-order flow field equations provides the bearing flow rate, radial/axial film forces and drag torque. Solutions to the first-order equations determine the rotordynamic force coefficients due to journal lateral and axial motions. Numerical predictions of load capacity and force coefficients for a 6 recess, spherical HJB in a LO_2 environment are presented for increasing values of the journal center radial and axial displacements. The results show that axial journal motions do not alter significantly the radial load capacity of the bearing. On the other hand, the spherical bearing geometry provides fluid film axial forces of a magnitude about 20% of the radial load capacity for the example analyzed. Fluid inertia effects, advective and centrifugal, are found to affect greatly the static and dynamic force performance of the bearing studied.

ACKNOWLEDGEMENTS

The generous support of the Rocketdyne Division of Rockwell International is gratefully acknowledged.

REFERENCES:

Adams, M., J.T. Sawicki, and R. Capaldi, 1992, "Experimental Determination of Hydrostatic Journal Bearing Coefficients," *Proceedings of the Institution of Mechanical Engineers*, Paper C432/145, International Conference in Vibrations in Rotating Machinery, IMechE 1992-6.

Artiles, A., Walowit, J., and W. Shapiro, 1982, "Analysis of Hybrid Fluid Film Journal Bearings with Turbulence and Inertia Effects," *Advances in Computer Aided Bearing Design*, ASME Publication No. G0020, pp. 25-51.

Chaomleffel, J, D. Nicholas, 1986, "Experimental Investigation of Hybrid Journal Bearings," *Tribology International*, Vol. 19, No. 5, pp. 253-259.

Childs, D., 1989, "Fluid-Structure Interaction Forces at Pump-Impeller-Shroud Surfaces for Rotordynamic Calculations," *ASME Journal of Vibration, Acoustics, Stress and Reliability in Design*, Vol.111, pp.216-225.

Constantinescu, V.N., and F. DiMofte, 1987, "On the Influence of the Mach Number on Pressure Distribution in Gas Lubricated Step Bearings," *Rev. Roum. Sci. Tech. - Mec. Appl.*, Tome 32, No 1, pp. 51-56.

Craighead, I.A., and P.S. Leung, 1992, "An Analysis of the Steady State and Dynamic Characteristics of a Spherical Journal Bearing with Axial Loading," *Proceedings of the Institution of Mechanical Engineers*, Paper C432/016, International Conference in Vibrations in Rotating Machinery, IMechE 1992-6, September, pp. 337-343.

Franchek, N., 1992, "Theory Versus Experimental Results and Comparisons for Five Recessed, Orifice Compensated, Hybrid Bearing Configurations," Texas A&M University, M.S. Thesis, TAMU Turbomachinery Laboratories.

Goenka, P.K., and J. Booker, 1980, "Spherical Bearings, Static and Dynamic Analysis Via the Finite Element Method," *ASME Journal of Lubrication Technology*, Vol. 102, 3, pp. 308-319.

Hall, K.R., P. Eubank, J. Holste, and K. Marsh, 1986, "Performance Equations for Compressible Flow Through Orifices and Other ΔP Devices: A Thermodynamics Approach," *AIChE Journal*, Vol.32, No. 3, pp. 517-519.

Hirs, G.G., 1973, "A Bulk-Flow Theory For Turbulence in Lubricating Films," *ASME Journal of Lubrication Technology*, pp. 135-146.

Kurtin, K., Childs, D., San Andres, L.A., and K. Hale, 1991, "Experimental versus Theoretical Characteristics of a High Speed Hybrid (combination Hydrostatic and Hydrodynamic) Bearing," *ASME Transactions*, Paper No. 91-Trib-35.

Mosher, P., 1993, "Experimental versus Experimental and Theoretical Characteristics of Five Hybrid (Combination Hydrostatic and Hydrodynamic) Bearing Designs for Use in High Speed Turbomachinery,"

M.S. Thesis, Texas A&M University.

McCarty, R.D., 1986, NBS Standard Reference Data Base 12, Thermophysical Properties of Fluids, MIPROPS 86, Thermophysics Division, Center for Chemical Engineering, National Bureau of Standards, Colorado.

Redecliff, J.M. and J.H. Vohr, 1969, "Hydrostatic Bearings for Cryogenic Rocket Engine Pumps," *ASME Journal of Lubrication Technology*, pp. 557-575.

San Andres, L.A., 1990, "Turbulent Hybrid Bearings with Fluid Inertia Effects", *ASME Journal of Tribology*, Vol. 112, pp. 699-707.

San Andres, L.A., 1991a, "Effect of Eccentricity on the Force Response of a Hybrid Bearing," *STLE Tribology Transactions*, Vol. 34, 4, pp.537, 544.

San Andres, L.A., 1992a, "Analysis of Turbulent Hydrostatic Bearings with a Barotropic Fluid," *ASME Journal of Tribology*, Vol. 112, 4, pp. 755-765.

San Andres, L.A., 1992b, "Analysis of Turbulent Bulk-Flow Hydrostatic Pad Bearings with a Barotropic Liquid, Cylindrical and Spherical Bearings," Turbomachinery Laboratory, Texas A&M University.

Scharrer, J.K., J. Tellier, R. Hibbs, 1991, "A Study of the Transient Performance of Hydrostatic Journal Bearings: Part I-Test Apparatus and Facility, Part II-Experimental Results," *STLE Tribology Transactions*, Preprint 91-TC-3B-2.

Scharrer, J.K., and T.W. Henderson, 1992a, "Hydrostatic Bearing Selection for the STME Hydrogen Turbopump," AIAA Paper 92-3283, 28th AIAA/SAE/ASME/ASEE Joint Propulsion Conference, Tennessee.

Scharrer, J.K., and L. San Andres, 1992b, "The Axisymmetrically Stepped, Orifice Compensated Hydrostatic Bearing," AIAA Paper 92-3405.

Sutton, R., J. Scharrer, and R. Beatty, 1991, "Hydrostatic Bearing for Axial/Radial Support," Official Gazette, U.S. Patent 5,073,036.

Yang, Z., San Andres, L., and D. Childs, 1992a, "Thermal Effects in Cryogenic Liquid Annular Seals, I: Theory and Approximate Solutions; II: Numerical Solution and Results", *ASME Transactions*, Papers 92-TRIB-4, 92-TRIB-5.

Yang, Z., 1992b, "Thermohydrodynamic Analysis of Cryogenic Hydrostatic Bearings in the Turbulent Flow Regime," Ph.D. Dissertation, Texas A&M University.

Table 1. Geometry and Operating Conditions of 6 recess, LO₂ Spherical Hydrostatic Journal Bearing.

Dimensions: Number of recesses $N_{rec} = 6$.

clearance, $c=101.6\mu\text{m}(0.004\text{ in})$; recess depth, $H_r=381\mu\text{m}(0.015\text{ in})$; $H_r/c=3.75$

Spherical: Diameter, $D^*=91.036\text{mm}(3.58\text{ in})$; Path Length, $S=71.50\text{mm}(2.815\text{ in})$;
 $DR=64.372\text{mm}(2.534\text{ in})$;
 Axial length, $L=64.372\text{mm}(2.534\text{ in})$; $L/D^*=0.707$, $R^*/c=448.0$
 Spherical angle $\gamma/2=45\text{ deg}$.

Recess: length $l=31.74\text{mm}(1.25\text{ in})$, circumferential length $\Theta_r=30.0\text{ deg}$.

journal and bearing surface conditions: smooth

Orifice $C_o=0.89$, diameter $d_o=2.377\text{mm}$ for concentric recess pressure ratio $pr=0.55$.

Recess edge (non-isentropic) coefficients $\xi_{11}=0.0$; $\xi_{12}=0.50$; $\xi_2=0.0$

Operating Parameters: rotational speed: 2,356 rad/s (22.5 Kcpm)
 Pressure supply, $P_s=15.16\text{ MPa}(2,200\text{ psia})$
 exit, $P_a=1.38\text{ MPa}(200\text{ psia})$

Fluid: LO₂ at 90K (162 R), $\mu_s=0.22454\text{E-}3\text{ Pa}\cdot\text{s}$, $\rho_s=1,172\text{ Kg/m}^3$
 $\mu_a=0.19813\text{E-}3\text{ Pa}\cdot\text{s}$, $\rho_a=1,144\text{ Kg/m}^3$
 $\beta=0.1696\text{-}8\text{ 1/Pa}=1\text{..}(85.52\text{ kpsi})\text{..}$

TYP Reynolds numbers:

$Re_{rec} = D_{sl} \omega R^* C / \mu_s = 56,900$

$Re_{axial} = m / (2\pi DR \mu_a) = 35,857$. Mass flow rate concentric = 2.8735 kg/s

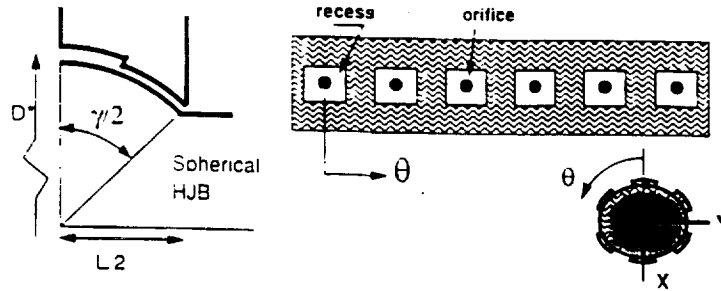


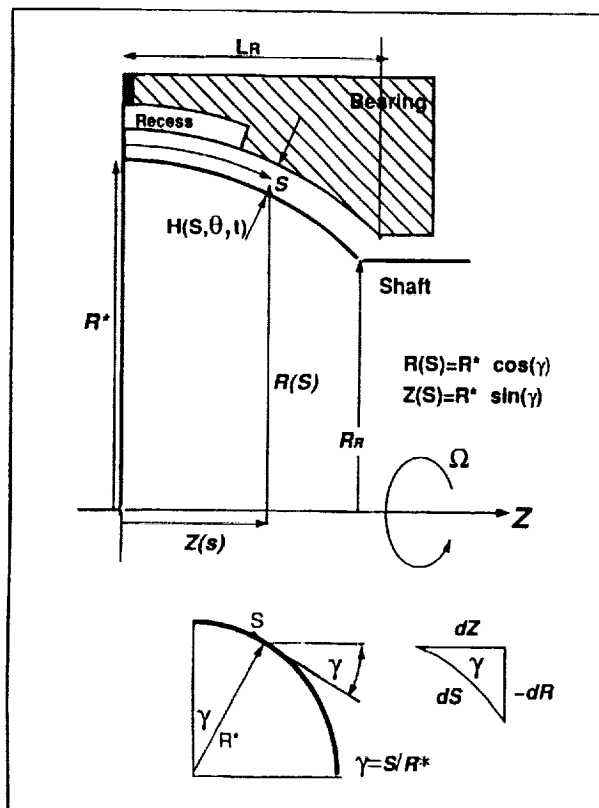
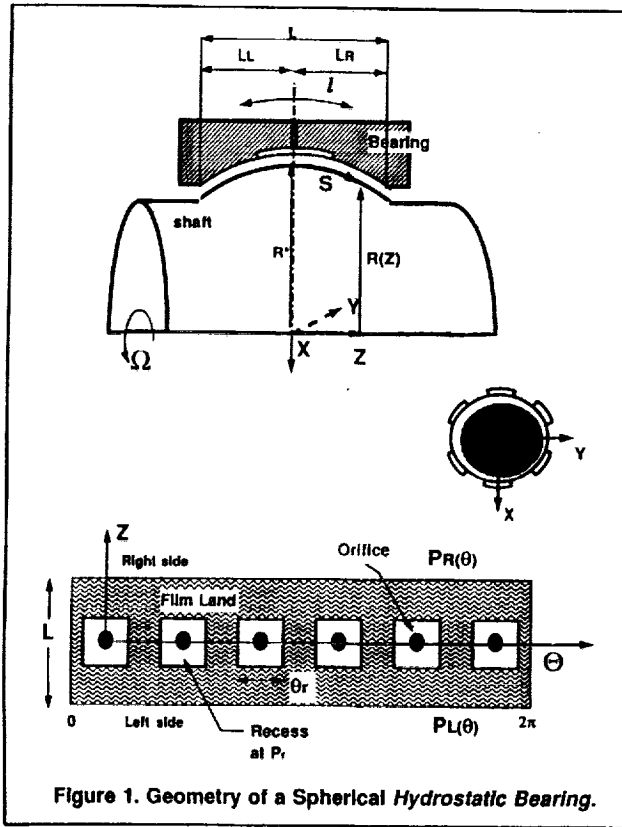
Table 2
Spherical hydrostatic bearing performance characteristics
Effect of Fluid Inertia

(a) Model with fluid inertia effects, $d_o=2.37\text{mm}$

Speed (Kcpm)	$P_r - P_a$ $P_s - P_a$	Mass flow (kg/s)	Torque (N·m)	$K_{XX} = K_{YY}$	$K_{XY} = -K_{YX}$	K_{ZZ}	$C_{XX} = C_{YY}$	$C_{XY} = -C_{YX}$	C_{ZZ}
				(MN/m)			(MN·s/m)		
0.00	0.4700	3.1314	0.000	179.32	0.00	6.82	151.90	0.00	19.30
12.50	0.4980	3.0160	2.833	229.20	112.30	6.74	153.60	16.86	19.50
22.50	0.5000	2.8735	5.980	240.90	198.90	6.43	165.30	25.50	19.70

(b) Model without fluid inertia effects, $d_o=2.37\text{mm}$

Speed (Kcpm)	$P_r - P_a$ $P_s - P_a$	Mass flow (kg/s)	Torque (N·m)	$K_{XX} = K_{YY}$	$K_{XY} = -K_{YX}$	K_{ZZ}	$C_{XX} = C_{YY}$	$C_{XY} = -C_{YX}$	C_{ZZ}
				(MN/m)			(MN·s/m)		
0.00	0.4157	3.2763	0.000	257.90	0.00	5.07	92.38	0.00	10.40
12.50	0.4302	3.2290	2.996	280.40	39.40	4.88	101.30	2.10	10.30
22.50	0.4632	3.1259	6.086	308.50	94.09	4.71	110.50	2.24	10.30



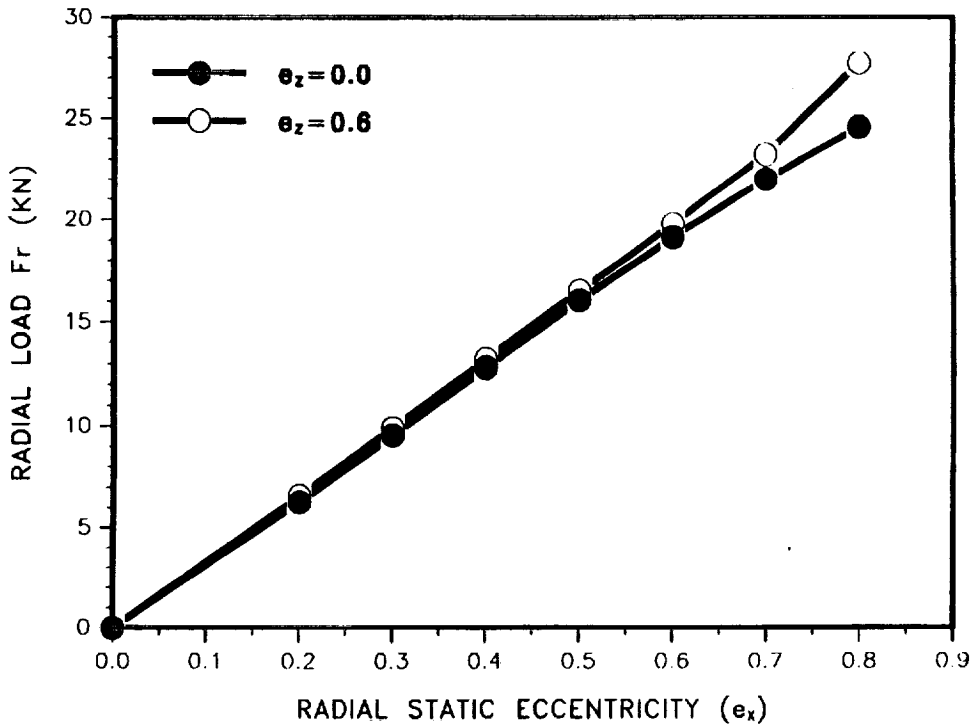


Figure 3. Radial Load vs. Journal radial eccentricity (ϵ_x) for journal axial displacements $\epsilon_z=0.0$ and 0.60

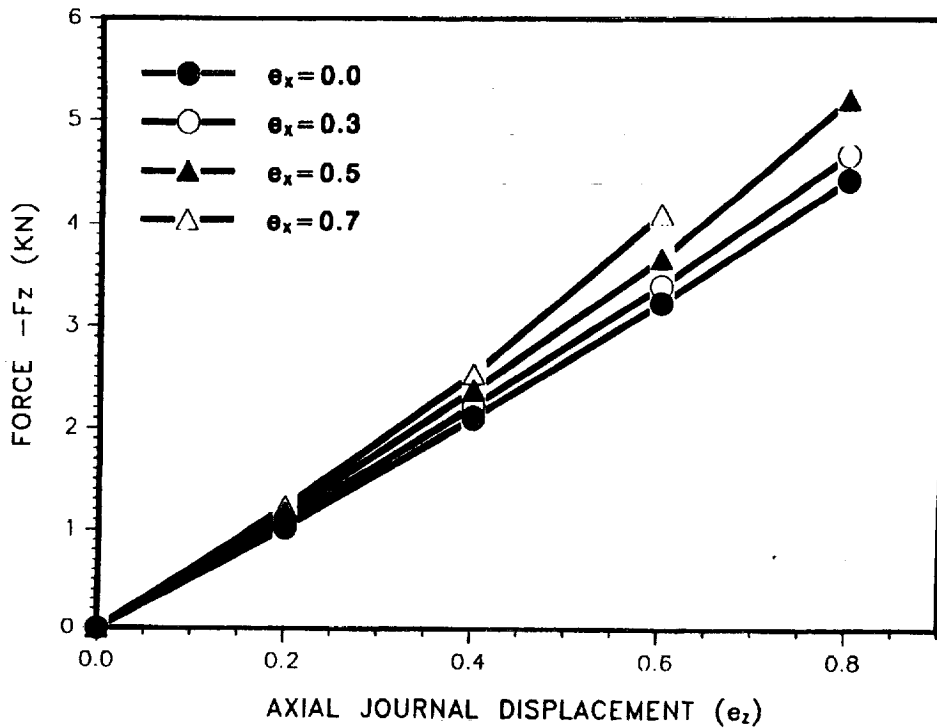


Figure 4. Axial force ($-F_z$) vs. journal axial eccentricity (ϵ_z) for increasing journal radial displacements ϵ_x .

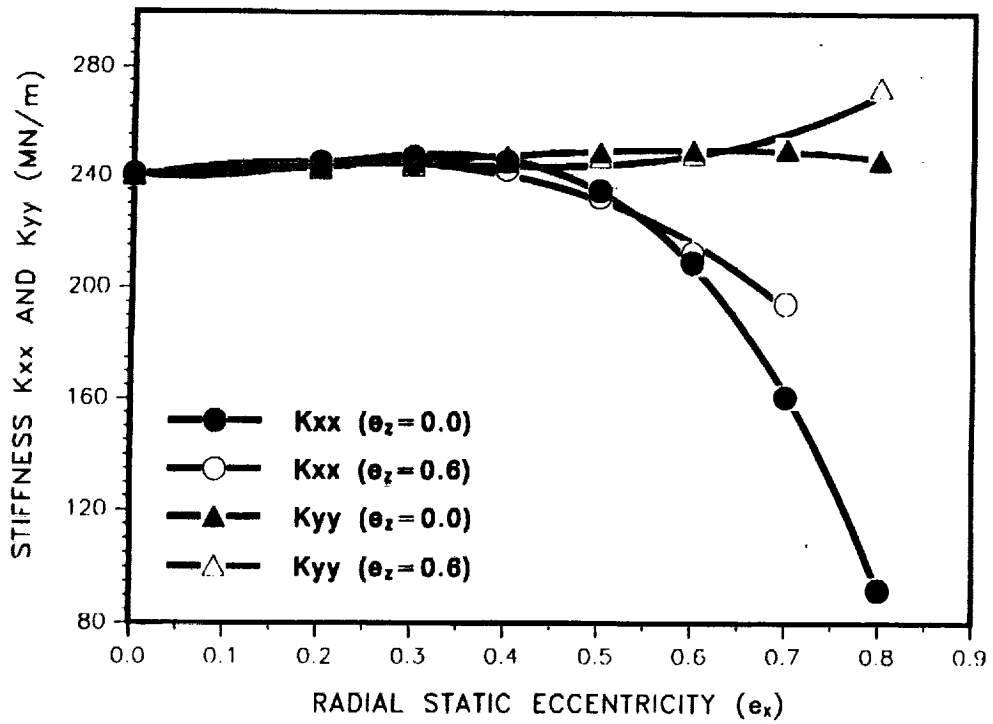


Figure 5. Lateral force stiffness coefficients (K_{xx} , K_{yy}) vs. journal radial eccentricity (e_x) for journal axial displacements $e_z=0.0$ and 0.60

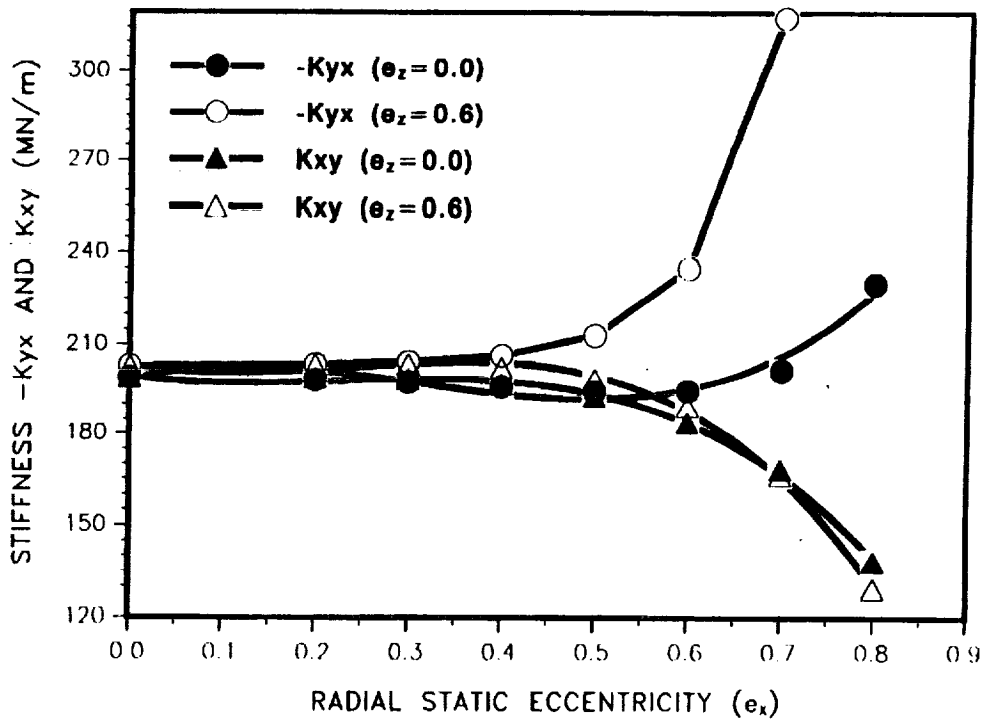


Figure 6. Lateral force stiffness coefficients ($-K_{xy}$, K_{yx}) vs. journal radial eccentricity (e_x) for journal axial displacements $e_z=0.0$ and 0.60

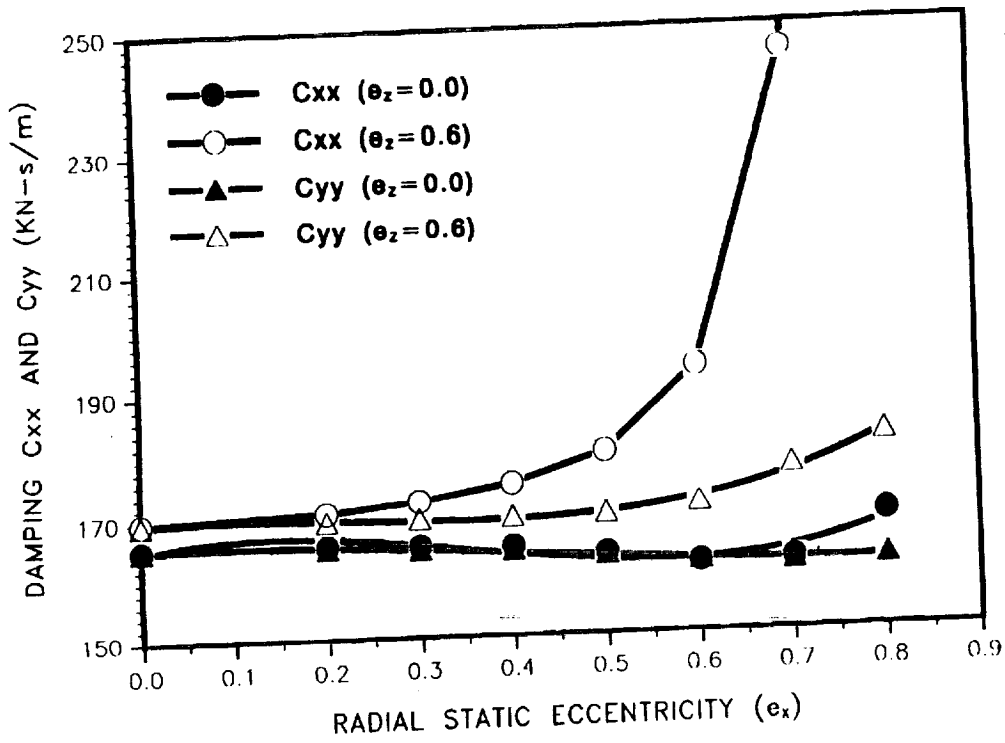


Figure 7. Lateral force damping coefficients (C_{xx} , C_{yy}) vs. journal radial eccentricity (e_x) for journal axial displacements $\epsilon_z=0.0$ and 0.60

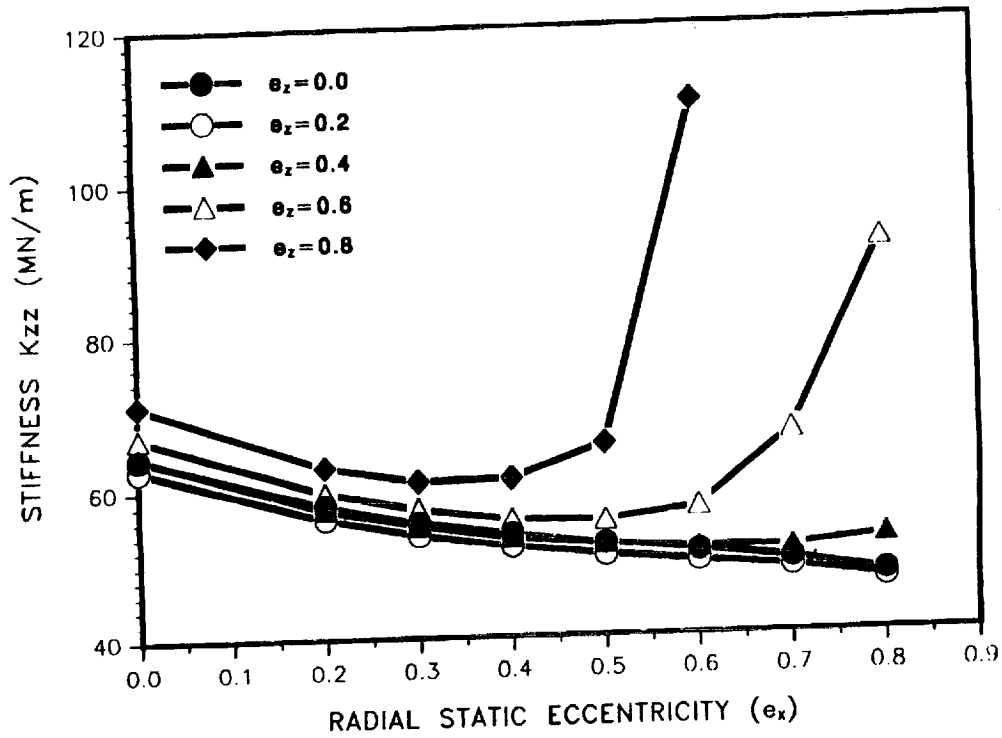


Figure 8. Axial force stiffness coefficient (K_{zz}) vs. journal radial eccentricity (e_x) for increasing journal axial displacements ϵ_z .

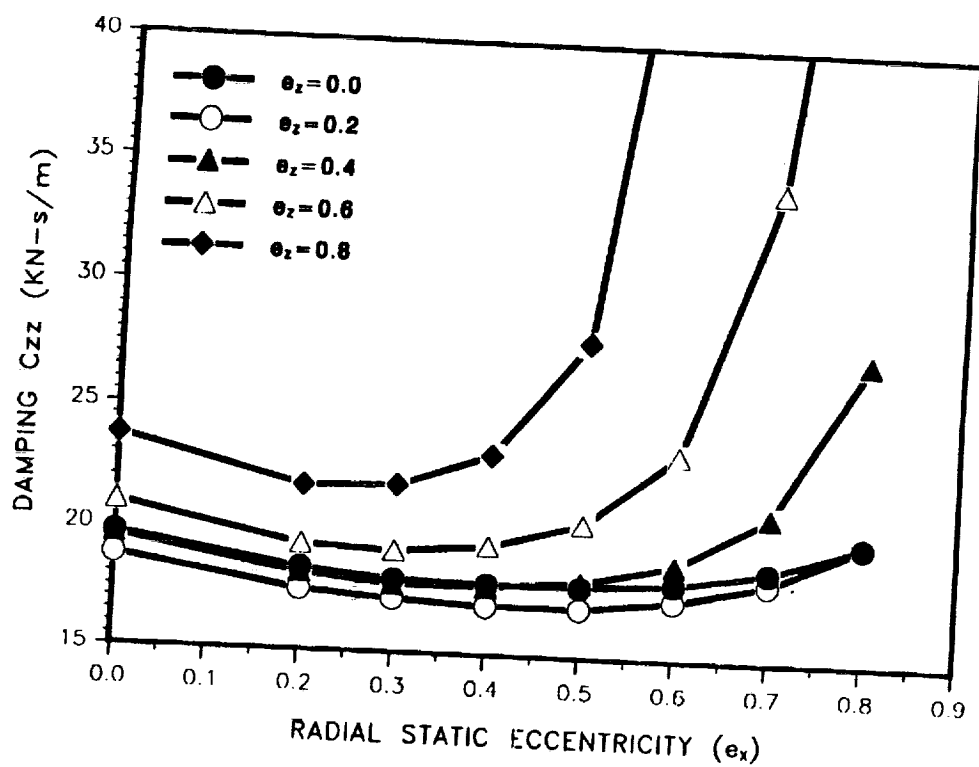


Figure 9. Axial force damping coefficient (C_{zz}) vs. journal radial eccentricity (e_x) for increasing journal axial displacements ϵ_z .